Macromolecules

pubs.acs.org/Macromolecules Article

The Importance of Morphology on Ion Transport in Single-Ion, Comb-Branched Copolymer Electrolytes: Experiments and Simulations

Sanket Kadulkar,[#] Zachary W. Brotherton,[#] Anna L. Lynch, Gabriel Pohlman, Zidan Zhang, Rudy Torres, Arumugam Manthiram, Nathaniel A. Lynd,* Thomas M. Truskett,* and Venkat Ganesan*

Cite This: *Macromolecules* 2023, 56, 2790−2800 Read Online

ACCESS | Metrics & More | Article Recommendations | Supporting Information

ABSTRACT: Single-ion conducting polymer electrolytes (SICPEs) offer high lithium transference numbers and desirable physical properties while maintaining moderate conductivities. Bottlebrush and comb-branched copolymer electrolytes are a particular architecture that offer modularity and increased ion solvation. Despite this promise, the ion transport in these systems is poorly understood. In this report, we investigated lithium-ion transport in comb-branched SICPEs using a combination of experiments and atomistic simulations. A series of solvent-free SICPEs were synthesized by copolymerization of poly(ethylene glycol) methyl ether acrylate (PEGMEA) with varying lithiated anionic groups in different ratios of the ionic species to the PEG side chain. Poly(Lithium 3-[(trifluoromethane) sulfonamidosulfonyl]propyl methacrylate-*co*-poly(ethylene glycol methyl ether acrylate)) (p(MPTFSI-*co*-PEGMEA) exhibited both highest ionic conductivity (on the order of 10^{-5} S/cm at room temperature) and degree of decoupling of ionic conductivity from polymer segmental dynamics. Simulations revealed that in electrolytes with low ion concentrations, Li^+ transport occurs through the vehicular codiffusion of lithium ions and the polyanions. In contrast, for higher anion compositions, the primary mechanism of Li^+ transport is through Li^+ ion hopping among the percolated ionic aggregates. Finally, we demonstrate that the behavior of ion hopping is influenced in a nonintuitive manner by the ion cluster morphology based on SICPE anion identity.

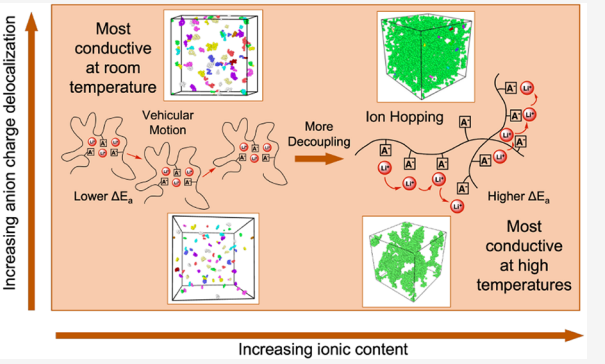

INTRODUCTION

Conventional organic liquid electrolytes offer high ionic conductivity which makes them suitable for lithium-ion batteries. Electrolytes with faster anion mobilities compared to those of the cations tend to form anion concentration gradients under discharge.[1] Such buildup of anion concentration gradients limits the energy density, charging and discharge rates of the battery, and can facilitate dendrite formation when employed with high-capacity Li metal anodes.[2−4] To overcome such challenges, single-ion conducting polymer electrolytes (SICPEs) have emerged as a potential solution.[5−7] In such electrolytes, immobilization of anions is achieved by covalently attaching the anion to the polymer backbone. However, the ionic conductivities of SICPEs are typically lower than those of conventional liquid electrolytes. Hence, there is a significant interest in strategies that can improve ionic conductivity in such electrolytes without negatively impacting their mechanical strength.[8−10]

In the above context, efforts have focused on weakening the interactions between the lithium ions and the immobile anionic groups to promote dissociation of lithium ions and thereby improve the ionic conductivity of SICPEs. To this end, the selection of anionic groups in SICPEs has been demonstrated to significantly affect ionic conductivity.[5−7] Specifically, SICPEs with sulfonylimide or borate anionic groups have been reported to exhibit superior ionic conductivities compared to those with sulfonate or carboxylate anionic groups due to the relatively higher delocalization of charge within the anionic groups.[11,12] Another strategy involves blending of SICPEs with polar, organic solvents (for example, ethylene carbonate, dimethyl carbonate, propylene carbonate, diethyl carbonate, and γ-butyrolactone) as plasticizers and also to enhance ion dissociation to improve the room temperature ionic conductivity.[13,14]

Recent studies have also focused on improving the ionic conductivity of SICPEs by lowering the glass transition

Received: December 12, 2022
Revised: January 31, 2023
Published: March 30, 2023

https://doi.org/10.1021/acs.macromol.2c02500
Macromolecules 2023, 56, 2790−2800

temperature (T_g) of the polymer to enhance ion transport driven by polymer segmental motion. Homopolymer SICPEs, in which every repeat unit in the polymer backbone harbors an anion, generally exhibit low ionic conductivity due to their high T_g values (>150 °C for lithium poly[(4-styrenesulfonyl)(trifluoromethanesulfonyl)imide]).[5−7] To this end, blending with poly(ethylene oxide) (PEO)[15,16] has been pursued as a straightforward solution to enhance the segmental motion of the SICPEs. However, despite the low glass transition temperatures, the high crystalinity of the PEO counteracts any gains in ionic conductivity at temperatures below the melting point of PEO (around 60 °C).[15,16]

In contrast to the above blending strategies, copolymerizing the backbones of the homopolymeric ionomers with short poly(ethylene glycol) (PEG) side chains has been demonstrated as an effective strategy to introduce flexible, low T_g PEO while suppressing the crystallinity of the polymer matrix to achieve ionic conductivities at room temperature of ca. 10^{-6} S/cm.[15,17−21] By controlling the composition of the copolymer, that is, the ratio of the number of PEO side chains to the number of anionic groups in the copolymer, the ion content of the electrolyte can be optimized. Previous experimental studies[17,20−22] have reported a decrease in the activation energy for ion transport with increasing fraction of PEO side chains in the copolymer (at relatively low ion content in the electrolyte), hinting at distinct mechanisms for ion transport at different ion compositions. Similarly, computational studies focused on copolymeric ionomers with varying length of PEO spacers in the backbone have also demonstrated the ion content to be a key design parameter influencing ionic conductivity.[23−30]

In this work, motivated by the above studies, we use a combination of experiments and simulations to investigate ion transport in single-ion conducting electrolytes based on comb-branched copolymers composed of poly(ethylene glycol) methyl ether acrylate (PEGMEA) and lithiated anionic groups. Specifically, we wish to determine whether the degree of decoupling of ionic conductivity from the polymer dynamics can be influenced by using SICPEs based on copolymers with low T_g, neutral side chains. To characterize the influence of the cation−anion interactions, electrolytes were prepared with three different anionic monomers: acrylic acetate (AA), 2-acrylamido-2-methylpropanesulfonate (AMPS), and methacrylate-propyl (trifluoromethanesulfonyl) imide (MPTFSI). The ion content was varied by changing the ratio of PEGMEA to lithiated anionic groups in the copolymer. Our results demonstrate that both ion content and anion identity significantly influence ionic conductivity. Complementary atomistic molecular dynamics (MD) simulations identify the transport mechanisms underlying the experimentally observed conductivity trends.

EXPERIMENTAL AND COMPUTATIONAL METHODS

Materials. Acrylic acid (Alfa Aesar, 99.5%, stabilizers added), acrylamidopropanesulfonic acid (Sigma-Aldrich, 99%), lithium methacryl(trifluoromethane sulfonyl imide) (Specific Polymers), poly(ethylene glycol)methyl ether acrylate Mn 480 (Sigma-Aldrich, stabilizers added), 2,2′-azobis(2-methylpropionitrile) (Sigma-Aldrich, 98%), 2-cyano-2-propyl dodecyl trithiocarbonate (Sigma-Aldrich, 97%), ethanol (Decon Laboratories, Inc.), dichloromethane (Fisher, stabilized), hexanes (Fisher), lithium hydroxide monohydrate (Acros Organics, 98%), deuterated dimethyl sulfoxide (Cambridge Isotope Laboratories, 99.9%), deuterated water (Cambridge Isotope Laboratories, 99.9%), and methyl acrylate (Acros Organics, 99%, stabilized)

General Synthesis of Polymer Materials. A generalized scheme for the synthesis of the polyelectrolytes is shown in Figure 1. The

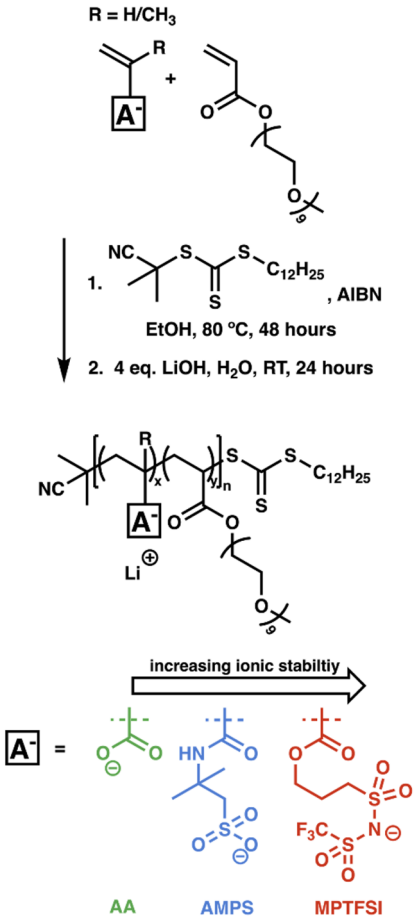

Figure 1. General synthesis scheme for PEG-oligomer graft copolymer electrolytes. Samples are denoted as PEGMEA$_y$/[anion]$_x$.

synthesis method was modified from existing procedures in literature.[17,31] Monomers, solvents, initiator, and the chain transfer agent were added in the desired quantity to a round-bottom flask charged with a stir bar and septa. The reaction vessel was sealed and degassed by bubbling nitrogen gas through the reaction solution for at least 20 min at room temperature. The reaction vessel was then submerged in a silicone oil bath preheated to 80 °C and maintained at this temperature for 48 h. Afterward, the reaction vessel was removed from the oil bath and rapidly cooled in liquid nitrogen for 10 min to quench remaining radicals. The solvent was removed via rotary evaporator, and the polymer was redissolved in dichloromethane. The polymer solution was precipitated in cold hexanes and redissolved in dichloromethane. This process was repeated twice more before the remaining solvent was removed via rotary evaporator and the polymer was dried in vacuo. The polymer was analyzed by NMR spectroscopy and differential scanning calorimetry.

To protonate the acidic polymers (those synthesized from conjugate acids of AA and AMPS), 2 g of the polymer was massed into an Erlenmeyer flask and dissolved in a small amount of deionized water. The anion contents of these polymers were calculated from their NMR spectra (Figures S18−S20 of the Supporting Information, SI). The polymers were treated with 4 equiv (relative to anion content) of 0.1 M lithium hydroxide solution in water and stirred at room temperature overnight. Excess LiOH was removed via dialysis against DI water (MWCO 3.5 kDa) for 3 days, with fresh water being replaced once daily. The water was removed via rotary evaporation and drying in vacuo at 90 °C overnight. Lithium-ion incorporation was confirmed by

https://doi.org/10.1021/acs.macromol.2c02500
Macromolecules 2023, 56, 2790−2800

flame test of the polymers, looking for a bright red flame characteristic of Li-ion containing compounds. LiOH removal was confirmed by redissolution of a small amount of lithiated polymer in water and pH analysis, in which polymers were very slightly basic due to the conjugate basicity of the polymer functional groups. The lithiated polymer salts were analyzed by NMR spectroscopy, electrochemical impedance spectroscopy, chronoamperometry, differential scanning calorimetry, and wide-angle X-ray scattering.

Characterization. Samples were prepared for NMR spectroscopy by dissolving 25 mg of polymer into 0.7 mL of deuterated solvent. Deuterated dimethyl sulfoxide was used when materials were soluble, and deuterated water was used otherwise. The samples were allowed to dissolve on a stir plate at room temperature for 1 h, then added to a sample tube. NMR spectra were collected from −2 to 14 ppm, with a pulse angle of 90° and a relaxation delay of 2 s. Sixteen individual spectra were collected for each sample and were averaged together to create each final spectrum. Peak integrals were compared between peaks related to the ionic repeat unit and that of the terminal methyl group of the polyethylene-glycol methyl ether macromonomer to measure anion-content. These peak integrals were also compared against the aliphatic hydrocarbon peak of the RAFT agent dodecyl group to determine the number-average molecular weight of the sample. The NMR spectra of the polymer electrolytes are shown in Figures S18−S20.

Samples were prepared for electrochemical impedance spectroscopy by heating to 90 °C and drying in vacuo for 12 h prior to sample cell assembly. Polymers were loaded into a small plastic washer 4.76 mm in diameter and 0.78 mm thick as a spacer. The polymer and spacer were loaded onto one gold electrode of a BioLogic CESH cell on a hot plate at 90 °C to decrease viscosity and ensure the spacer fills completely. A slight excess of polymer was added to also fill the washer fully. The other gold electrode plate was attached, and the cell was allowed to anneal on a hot plate at 90 °C for 1 h. The real and imaginary components of the impedance of the assembled cell were measured as a function of frequency of alternating current from 1 MHz to 100 mHz at 10 points per decade using a BioLogic MTZ-35 and ITS-e. At each frequency, 10 data points were collected and averaged. The frequencies were swept across a temperature range of either 30−90 °C or 30−150 °C in both the heating and cooling thermal directions. The raw electrochemical impedance spectra are shown for each polymer electrolyte in Figures S24−S26. Conductivities were calculated at each temperature for each polyelectrolyte from the frequency trace by extrapolating the characteristic semicircle to the real resistance axis and equating the intercept value as the characteristic resistance of the sample cell. The conductivity was then calculated using this characteristic resistance and the geometry of the sample cell. Samples were prepared for chronoamperometry under Argon by sealing roughly 30 mg of the polymer electrolyte between two clean lithium chip electrodes in a swagelok-type stainless steel cell. The electrodes were separated by a 7.11 mm inner diameter × 0.762 mm thick PTFE washer. The cell was allowed to anneal at room temperature for 1 h before chronoamperometry. Using a BioLogic VMP-3e, a potential of either 10 mV or 50 mV was applied across the cell. The current through the cell was measured as a function of time. Data were collected for 12 h while the voltage was applied. The average current between 9 and 12 h was used as the steady state current. Impedance spectra of the cell were collected before and after the polarization to measure the initial and final resistance. The extracted parameters were used in the Bruce and Vincent method[32] using eq 1 to determine t_{Li+}. All chronoamperometry trials were conducted in triplicate. Due to low conductivities of these polymer electrolyte samples, the current measured during polarization was not significantly greater than the detection limit of the instrument. Thus, all chronoamperometry data and lithium transference number results were unreliable and omitted from this report.

$$t_{Li+} = \frac{I_{ss}^{*}(\Delta V - I_0 R_0)}{I_0^{*}(\Delta V - I_{ss} R_{ss})} \quad (1)$$

Samples were prepared for differential scanning calorimetry by drying overnight at 90 °C in vacuo. 2−8 mg of polymer electrolyte was massed out into a DSC pan which was hermetically sealed. Differential scanning calorimetry traces were collected from −40 °C to 150 °C and cycled 3 times. Glass transition temperature was calculated by TRIOS software analysis using the average inflection point temperatures of the heating traces as the glass transition temperature. Raw DSC data are shown for each polymer electrolyte in Figures S21−S23.

Samples were prepared for X-ray scattering tests by drying overnight in vacuo heated at 90 °C. Samples were placed into a small metal washer and sealed on both sides with low-scatter Kapton tape. Samples were aligned to a 45 W dual aperture X-ray beam and the scattering profile $I(q)$ was collected from q = 0.01/Å to 0.2/Å.

Simulation Details. We used all-atom MD simulations to probe the mechanisms underlying the experimental observations. Explicitly, we used the following interaction potential between atoms:

$$U = \sum_r U_{bond}(r) + \sum_\theta U_{ang}(\theta) + \sum_\phi U_{dih}(\phi) + \sum_\phi U_{imp}(\phi) + \sum_{ij} U_{nb}(r_{ij}) \quad (2)$$

where the bonds and angles were modeled using harmonic potentials of the form $U_{bond}(r) = k_r(r - r_0)^2$ and $U_{ang}(r) = k_\theta(\theta - \theta_0)^2$. Proper dihedrals were modeled using the Optimized Potentials for Liquid Simulations (OPLS)-style potential:

$$U_{dih}(\phi) = \frac{1}{2}\sum_{n=1}^{4} K_n[1 + (-1)^{n+1}\cos(n\phi)] \quad (3)$$

The energy contributions from the improper dihedrals are represented by the Consistent Valence Force Field (CVFF) form, given by $U_{imp} = K[1 - \cos(2\phi)]$. The nonbonded interactions (U_{nb}) consist of the following Lennard−Jones (LJ) pair potentials and Coulombic pair interactions:

$$U_{nb}(r_{ij}) = \left\{4\epsilon_{ij}\left[\left(\frac{\sigma_{ij}}{r_{ij}}\right)^{12} - \left(\frac{\sigma_{ij}}{r_{ij}}\right)^{6}\right] + \frac{Cq_iq_j}{r}\right\} f_{ij} \quad (4)$$

where $\epsilon_{ij} = \sqrt{\epsilon_i \epsilon_j}$ and $\sigma_{ij} = \sqrt{\sigma_i \sigma_j}$. The parameter f_{ij} was set to zero if atoms i and j are connected via a bond or angle, 0.5 for atoms that are in the 1−4 positions of the same proper dihedral, or unity for all other cases. The force fields for the atomistic MD simulations were adapted from the OPLS-all atom (OPLS-AA) optimized potential for liquid simulations.[33−35] Additionally, the partial charges for the MPTFSI anion and the PEGMEA side chains were extracted using density functional theory (DFT) calculations at B3LYP/6-311g** level of theory[36−38] using the Gaussian16 package.[39]

We performed the atomistic MD simulations using the LAMMPS (Large-scale Atomic/Molecular Massively Parallel Simulator) MD package.[40] The simulation box consisted of 40 random copolymers, each with a degree of polymerization of 40. To maintain charge neutrality, the concentration of Li^+ ions in the simulation box was maintained proportional to the mole fraction of anion in the copolymer (x_{anion}). The MD trajectories were generated at 600 K to facilitate faster ion mobilities and obtain better statistics in reasonable simulation time scales. Additional simulation details pertaining to the force fields, methodology, and subsequent analyses are presented in SI Section S1.1,S1.2.

RESULTS AND DISCUSSION

Ionic Conductivities. Figure 2a presents the experimental results for ionic conductivities measured as a function of temperature (30−90 °C) for copolymer electrolytes with different anionic repeat units and ion compositions. The experimental ionic conductivity measurements for electrolytes containing AA and AMPS were limited only to low ion contents (x_{anion} < 0.22) as these electrolytes with high ion contents formed brittle, ionic-crystalline solids which did not allow for sufficient contact with the sample cell electrodes. The

https://doi.org/10.1021/acs.macromol.2c02500
Macromolecules 2023, 56, 2790−2800

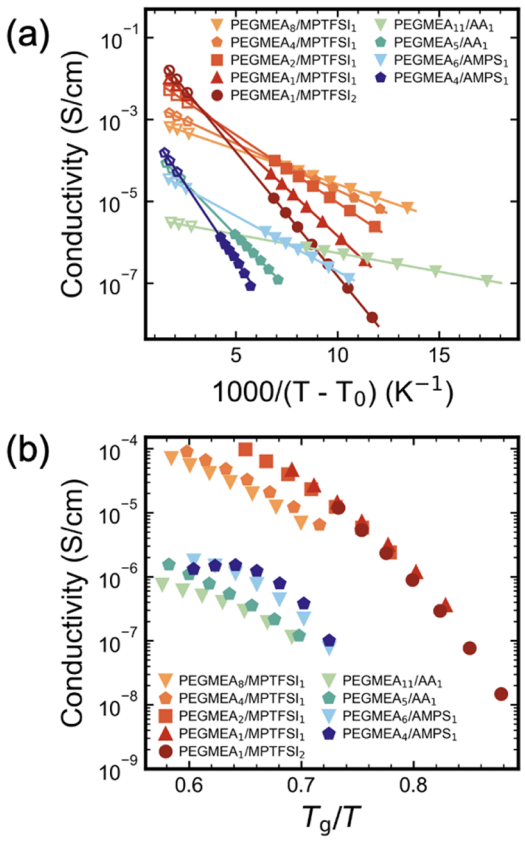

Figure 2. Experimental ionic conductivity of electrolytes on varying anion chemistry and copolymer composition (a) Conductivity data (solid symbols) collected from 30 to 150 °C. Lines are fit of eq 5. The open symbols represent the extrapolated conductivity at 600, 700, and 800 K predicted by the fit curves. (b) Conductivity as a function of T_g/T.

temperature-dependent conductivity data was observed to be well fit by the Vogel−Tammann−Fulcher (VTF) equation:

$$\sigma = A \exp\left(-\frac{E_a}{R(T - T_0)}\right) \tag{5}$$

with A, E_a, and T_0 being the fitting parameters.[41] The ionic conductivities for different electrolyte samples at room temperature (30 °C) along with their activation energies for ion transport (E_a), T_g values and NMR determined molecular weight are listed in Table 1.

For a specified anion chemistry, the measured ionic conductivities were observed to decrease with increasing ion content. Such trends were in agreement with those reported in previous experimental studies on single-ion conducting copolymers.[17−21] Interestingly, the activation energies for ion transport, quantified by the slope of the VTF fit curves, were observed to increase monotonically with increasing ion content. As a result, the *fit* values for ionic conductivity at higher temperatures (600 K) were seen to increase with increasing Li^+ ion concentration. Furthermore, the different E_a values for electrolytes with different ion contents hint at potentially distinct mechanisms for ion transport at varying ion contents. To render explicit the influence of ion content on the extent of decoupling between ionic conductivity and polymer segmental dynamics, we present results for ionic conductivity displayed as a function of the inverse glass-transition-normalized temperature T_g/T (Figure 2b). Since we probed the same range of temperatures for the different systems, the set of normalized temperatures for the different materials do not wholly overlap in the domain investigated. However, at a specified T_g/T and similar ion contents, the conductivity values are seen to be larger for electrolytes with the MPTFSI anion, indicating a greater degree of decoupling of ion transport from polymer dynamics.

In the following section, we discuss the results of atomistic MD simulations carried out to understand the mechanisms underlying the above experimental observations. Since the simulations model the system at 600 K (to alleviate the slow dynamics accompanying lower temperatures), we focus on the following questions arising from the extrapolation of the experimental results to the higher temperatures explored in the simulations:

1. Are there distinct mechanisms underlying ion transport as a function of ion content?
2. What are the origins of the influence of the anion chemistry?

Mechanisms of Ion Transport. To understand the mechanisms of ion transport leading to the above experimentally observed trends, atomistic MD simulations were performed to characterize the dynamics of ions. We sought to quantify the mobility of ions using their self-diffusivity via the Einstein relation,

$$D_i = \lim_{t\to\infty} \frac{1}{6t}\langle(\boldsymbol{r}_i(t) - \boldsymbol{r}_i(0))^2\rangle \tag{6}$$

where $\langle(\boldsymbol{r}_i(t) - \boldsymbol{r}_i(0))^2\rangle$ is the mean squared displacement (MSD) of ion type i at time t. The raw MSDs for both Li^+ and

Table 1. Ratio of Ethylene Oxide Units to Li^+ Ions, Ambient Temperature Ionic Conductivities, Activation Energy for Ion Transport, and Glass Transition Temperature T_g for Different Electrolyte Samples

sample	Li^+/EO	M_n^{NMR} (kg/mol)	log σ_{25}	E_a (kJ/mol)	T_g (K)
$PEGMEA_8/MPTFSI_1$	0.0139	25.7	−5.15	3.26	212
$PEGMEA_4/MPTFSI_1$	0.0278	27.1	−5.19	4.36	217
$PEGMEA_2/MPTFSI_1$	0.0556	18.2	−5.62	6.34	236
$PEGMEA_1/MPTFSI_1$	0.111	16.2	−6.44	8.86	251
$PEGMEA_1/MPTFSI_2$	0.222	25.4	−7.83	11.63	266
$PEGMEA_{11}/AA_1$	0.0101	31.9	−6.94	1.74	209
$PEGMEA_5/AA_1$	0.0222	43.5	−6.92	9.83	211
$PEGMEA_6/AMPS_1$	0.0185	19.7	−6.89	5.19	219
$PEGMEA_4/AMPS_1$	0.0278	19.7	−7.08	14.29	219

https://doi.org/10.1021/acs.macromol.2c02500
Macromolecules 2023, 56, 2790−2800

the anions can be found in Figure S4. The simulated ionic conductivity σ_{NE} was then computed using the equation

$$\sigma_{NE} = \frac{e^2}{Vk_BT}(N_{cat}z_{cat}^2D_{cat} + N_{an}z_{an}^2D_{an}) \quad (7)$$

where k_B, N_i, and V are the Boltzmann constant, the number of ion type i, and the system volume, respectively. We note that the Nernst−Einstein conductivity neglects the contribution of the correlated motion of ions to the ionic conductivity.

We display the simulation results for ionic conductivity in Figure 3a. We observed that the trends for the simulated

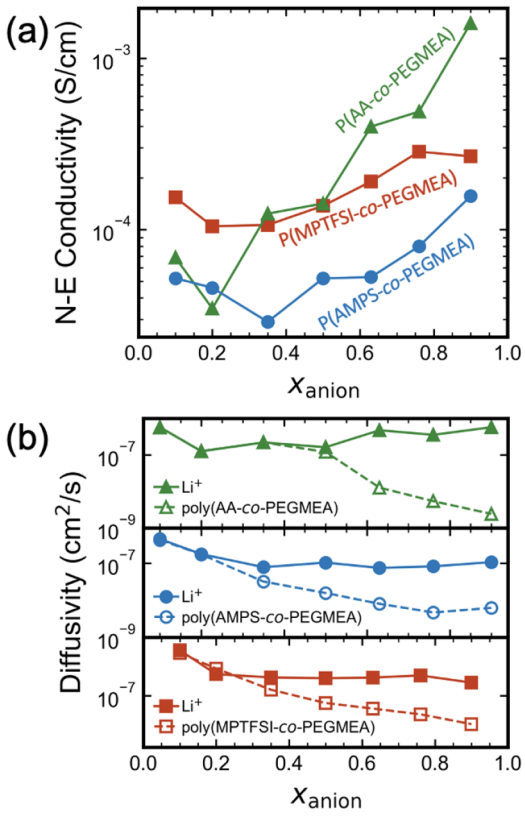

Figure 3. Simulated ion transport properties of electrolytes at 600 K. (a) Nernst−Einstein conductivity versus copolymer composition. (b) Li^+ and polyanion diffusivities at different copolymer compositions.

Nernst−Einstein ionic conductivities were qualitatively consistent with those extrapolated from experiments using the VTF fit curves. Explicitly, at low ion contents, the electrolytes containing MPTFSI exhibited higher ionic conductivities than those with other anion chemistries considered in this study. Further, with increasing ion content, the simulated ionic conductivities, except for a slight initial decrease, exhibited a monotonic increase as seen from the experimental conductivities (extrapolated to higher temperatures) (Figure 2a). Significantly, the increase in simulated ionic conductivities at higher ion contents (although not accessible experimentally) was found to be more prominent for the electrolytes containing AA compared to those with MPTFSI or AMPS.

To understand the origins of the above conductivity trends, we compare the results for the diffusivities of the polyanions and the Li^+ ions as a function of ion concentration in the electrolyte. From the results presented in Figure 3b, we observed that the polymer dynamics monotonically slowed with increasing ion content. Such trends for polymer dynamics are consistent with the experimental observations of monotonically increasing T_g values as a function of ion content (Table 1). In contrast, two distinct trends were observed for Li^+ diffusivities as a function of ion concentration. At low ion composition, the Li^+ diffusivity decreased initially and followed the trend for polymer diffusivities. However, beyond a critical ion composition, the Li^+ diffusivity approached a constant value for electrolytes with AMPS and MPTFSI, and exhibited a slight increase for electrolytes with AA, suggesting a more decoupled system at high anion content. While these data may inspire an investigation of lithium transference number as a function of anion composition, we note that these are binary systems (consisting only of cations and anions) in which the true lithium transference number should be determined by the ratio of the molar masses of the anionic repeat unit to that of the lithium ion.[42,43] This would hypothetically result in a lithium transference number above 0.98 in all cases. While we believe this is likely to be the true transference number, any measurements we performed lacked sufficient current and precision to verify this result.

Before we discuss the origins of the Li^+ diffusivity trends, we first rationalize the observed trends for polymer mobility with increasing ion content. In this context, we note that a number of previous computational studies[24−27,29,44] on ionomeric systems have observed the formation of ionic clusters of the mobile and the grafted ions, and attributed the slower polymer dynamics to the formation of such aggregates. Within this framework, we hypothesize that increasing ion content would lead to an increase in ionic aggregation thereby leading to slower polymer segmental dynamics (that is, the ionic aggregates can be envisioned as physical cross-links).[23,45]

To test our above hypothesis, we first observed based on the coordination behavior of Li^+ ions (Figures S5−S8) that the Li^+ ions were primarily bound to the oxyanions in the anionic groups. On the basis of this, the ions were assumed to be associated if their centers of mass distance was found to be within a cutoff distance of 3.0 Å corresponding to the first coordination shell of the Li^+−O (anion) radial distribution functions. Using such a measure, we quantified the ionic aggregate size distribution and the average aggregate size as a function of the ionic content $\bar{n}$.[46] From the results in Figure 4, the average ionic aggregate size monotonically increased with ion content. Together, these characteristics serve to rationalize

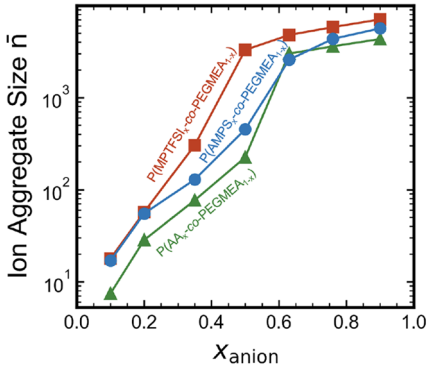

Figure 4. Simulated average ionic aggregate size as a function of copolymer composition. Electrolytes corresponding to different anion chemistries are represented as AA (green ▲), AMPS (blue ●), and MPTFSI (red ■).

https://doi.org/10.1021/acs.macromol.2c02500
Macromolecules 2023, 56, 2790−2800

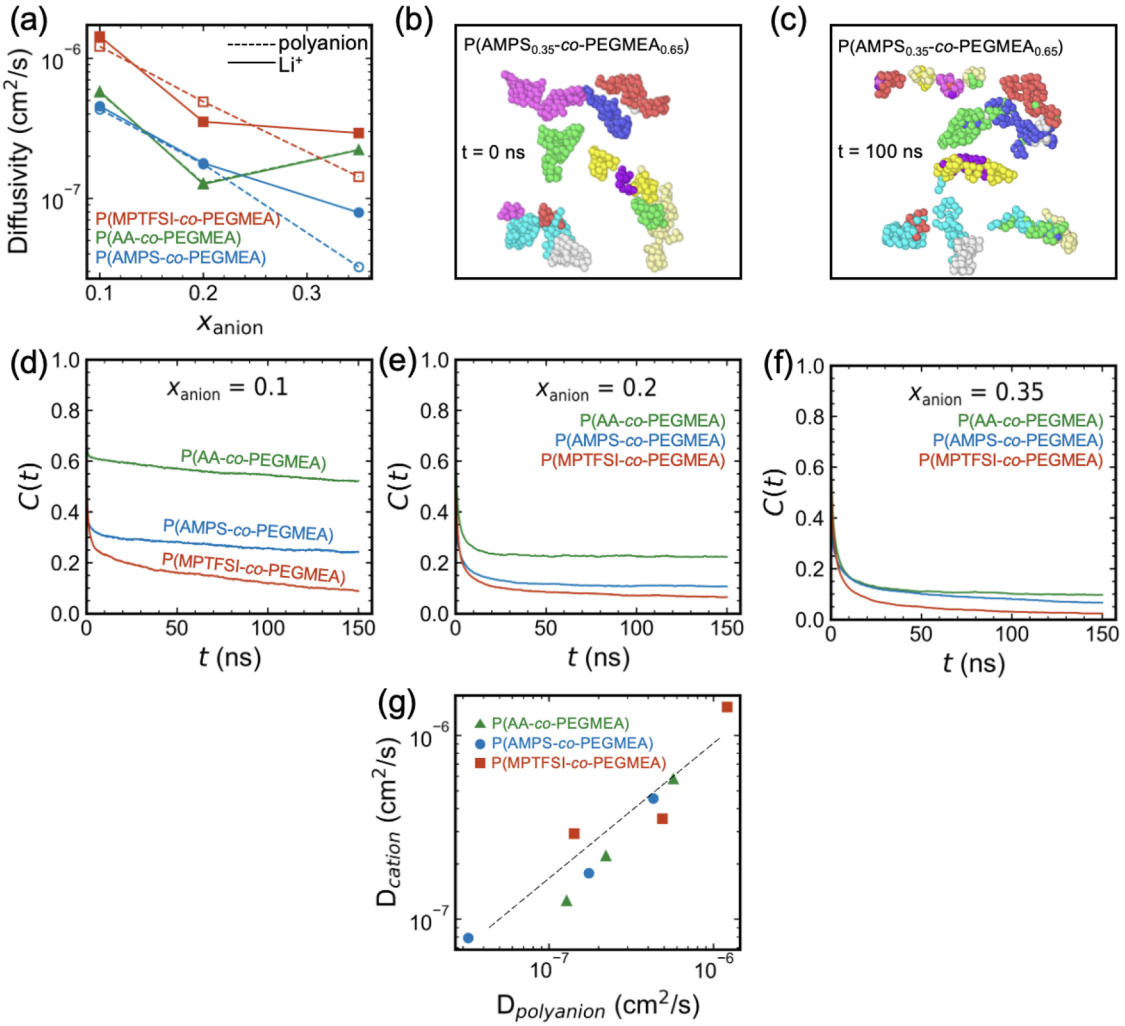

Figure 5. Simulation data for the lower ion content regime. (a) Li^+ (solid symbols) and polyanion (open symbols) diffusivities in lower ion content regime. Snapshots of MD simulations for system with AMPS (x_{anion} = 0.35) at time (b) t = 0 and (c) t = 100 ns. Different colors represent distinct aggregates at t = 0. All ions keep the same color at the later time. Li^+−O (anion) association autocorrelation functions for the electrolytes with (d) x_{anion} = 0.1, (e) x_{anion} = 0.2, and (f) x_{anion} = 0.35. Systems with different anion chemistries are represented as AA (green), AMPS (blue), and MPTFSI (red). (g) Correlation between Li^+ and polyanion diffusivities in lower ion content regime.

the observed decrease in polymer mobility with increasing ion content.

Li^+ Transport Mechanisms in Low Ion Concentration Regime. At low ion contents (x_{anion} < 0.35), the trend for Li^+ diffusivity was seen to mirror that of the polymer mobility (Figure 5a). In this regime, the visualization of the corresponding simulation snapshots at different times (Figure 5b,c), suggested that the Li^+ ions stay bound to the oxygens in the anionic groups for a long time. To quantify the association characteristics of Li^+−O (anion) association, we computed the ion-pair association autocorrelation function defined as

$$C(t) = \frac{\langle h(t_0)h(t_0 + t)\rangle}{h} \tag{8}$$

where $h(t)$ takes a value of 1.0 if the Li^+−O (anion) association is present at time t and zero otherwise. In essence, $C(t)$ represents the probability of two ions being associated at time t, given they were associated at time t = 0. The results for ion-polymer association time scales are displayed in Figure 5d−f. Therein, at the low ion contents (x_{anion} < 0.35), the $C(t)$ does not decay to zero even after 150 ns. This persistence confirmed the long-lived nature of Li^+−O (anion) association.

The visualization of the corresponding simulation snapshots at different times (Figure 5b,c), combined with the fact that the Li^+ ions stay bound to the oxygens in the anionic groups for a long time, suggests that the lithium-ion movement occurs by a combination of vehicular motion of the ion pair and rearrangement of ionic aggregates occurring by the process of merging and breaking up.[23−30] Given the above observations, the initial slight decrease in ionic conductivity with ion content (Figure 3a) can be understood as a consequence of the corresponding decrease in the polymer mobility (Figure 3b). Within this reasoning, the higher ionic conductivity for electrolytes containing MPTFSI can be attributed to the faster dynamics of the copolymer (Figure 5a). The faster rearrangement physics are also reflected in the faster decay of the ion-pair association autocorrelation functions for MPTFSI copolymers (Figure 5d−f). These faster dynamics and shorter ion-pair association lifetimes explain the order-of-magnitude increase in room temperature conductivity of MPTFSI copolymers over AA and

https://doi.org/10.1021/acs.macromol.2c02500
Macromolecules 2023, 56, 2790−2800

AMPS copolymers in the low-ion content regime seen in Figure 2.

Next, we investigated the origins for decoupling of ion transport from polymer dynamics as a function of anion chemistry in the low anion content regime (Figure 2b). Since the Li^+ transport was found to be significantly coupled to the polymer dynamics in this regime, we expected the extent of decoupling to be related to the correlation between the simulated cation and polymer diffusivities in the low anion content regime. As shown in Figure 5g, we observe that the dependence of Li^+ transport on polymer mobility was much weaker for electrolytes containing MPTFSI (Coefficient of determination $R^2 = 0.85$) compared to those with AMPS ($R^2 = 0.97$) or AA ($R^2 = 0.99$). These trends are in agreement with our experimental findings of MPTFSI-containing electrolytes exhibiting the highest degree of decoupling in the low anion content regime (Figure 2b).

The above trends can be understood by noting that smaller ion-polymer association time scales are likely to result in faster local ion exchanges within the discrete ionic aggregates and maximize the extent of Li^+ transport occurring by structural rearrangement of the ionic aggregates. This is expected to lead to increased decoupling of Li^+ transport from polymer dynamics. The results presented in Figure 5d–f show that in agreement with our hypothesis, the Li^+ ions dissociate from the anions faster in electrolytes with MPTFSI compared to those with AMPS and AA, thus resulting in stronger decoupling for MPTFSI-containing electrolytes. This argument is further supported by visualization of the simulation snapshots demonstrating ionic aggregates at different times for electrolytes with different anionic units (Figures S9–S12). Specifically, we observe the extent of structural rearrangement of ionic aggregates to be strongest in electrolytes containing MPTFSI.

To understand the factors determining ion-pair association time scales for different anionic groups, we focus on the partial charges of the oxyanions (calculated to be $-0.79e$ for AA, $-0.68e$ for AMPS and $-0.64e$ for MPTFSI) which influence the electrostatic interactions between the Li^+-anion pair. We observe that the frequency of ion-pair dissociation increases as ion-pair electrostatic interactions weaken. These results help rationalize the experimentally observed trend pertaining to the influence of anion chemistry on the extent of decoupling of ion transport from polymer dynamics in electrolytes with *low ion concentrations* (Figure 2b).

Li^+ Transport Mechanism in High Ion Concentration Regime. In contrast to the low ion content regime, the trends for Li^+ mobility significantly deviate from that of the polymer mobility for electrolytes with high ion content. Explicitly, Li^+ diffusivities increase with ion content (for electrolytes containing AA) or approach a constant value (for electrolytes with AMPS and MPTFSI) despite a decreasing trend for polymer mobility. Further, such electrolytes with high ion contents are seen to exhibit almost single ion conductivity since the Li^+ mobilities are roughly an order of magnitude higher than those of their respective polyanions.

Simulation results demonstrate that even at these higher ionic contents, a majority of the Li^+ ions are coordinated to the oxyanions (Figures S5–S8). To rationalize the observed decoupling between ion motion and polymer dynamics, we hypothesize that the long-range movement of Li^+ ions occurs by hopping motion along the anionic groups within and between the ionic aggregates. Since the ion-hopping mode of Li^+ transport does not necessarily rely on polymer motion, such an ion transport mechanism will lead to a decoupling between ion transport and polymer dynamics.

To validate the above hypothesis, we probed whether at high ion contents, the Li^+ diffusivities exhibit a correlation with the frequency of Li^+ ion hops between the anion sites. Toward this objective, we computed the average ion-pair association lifetime by fitting a stretched exponential of the form $\exp(-(t/\alpha)^{\beta})$ to the association autocorrelation functions (eq 8). The average association lifetimes τ_c were then calculated as

$$\tau_c = \alpha\Gamma\left(1 + \frac{1}{\beta}\right) \tag{9}$$

In Figure 6, we display the Li^+ diffusivities and the corresponding average ion-pair association lifetimes for the different anions and compositions at higher ionic contents. Therein, a universal correlation between the Li^+ diffusivities and the ion pair average lifetimes was observed. The latter confirms that the mechanism for Li^+ transport in the high ion content regime to be hopping along the anionic groups relatively immobilized by the polymer backbone. These results support the existence of different mechanisms for ion transport in the low and high ion content regime, which were consistent with the experimentally observed dependence of activation energies on the ion content (Figure 2a and Table 1).

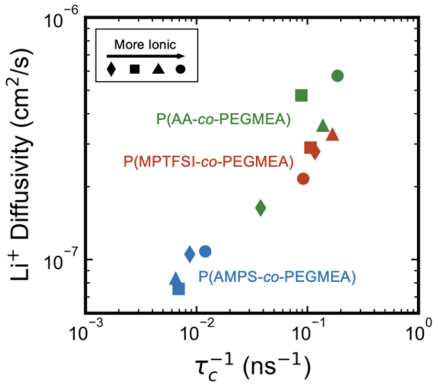

Figure 6. Simulated Li^+ diffusivity versus average ion-pair association lifetime to demonstrate a universal relationship for systems with higher ion content. Systems with different anion chemistries are represented as AA (green symbols), AMPS (blue symbols), and MPTFSI (red symbols). Different copolymer compositions are represented as x_{anions} = 0.5 (diamonds), x_{anions} = 0.63 (■), x_{anions} = 0.76 (▲), and x_{anions} = 0.9 (●).

Next, we focus on the influence of anion identity on ionic conductivity in the higher ion content regime. We note that the ion pair average lifetimes are expected to be influenced by both the interaction strength of the ion pairs and the ionic aggregate morphology. Explicitly, a less delocalized oxyanion typically leads to increased ion pair lifetimes and was thereby expected to result in slower Li^+ transport. However, contradicting such an intuition, the simulated results for Li^+ diffusivities (Figure 3b) revealed that the electrolytes containing AA exhibit highest Li^+ mobilities despite the strongest ion-pair electrostatic interactions.

To explain the observed dependence of the simulated ionic conductivity on anion chemistry in the higher ion content regime, we examined the corresponding ionic aggregate morphologies for electrolytes with different anionic species. From visual inspection of the simulation snapshots (Figure 7a–

https://doi.org/10.1021/acs.macromol.2c02500
Macromolecules 2023, 56, 2790−2800

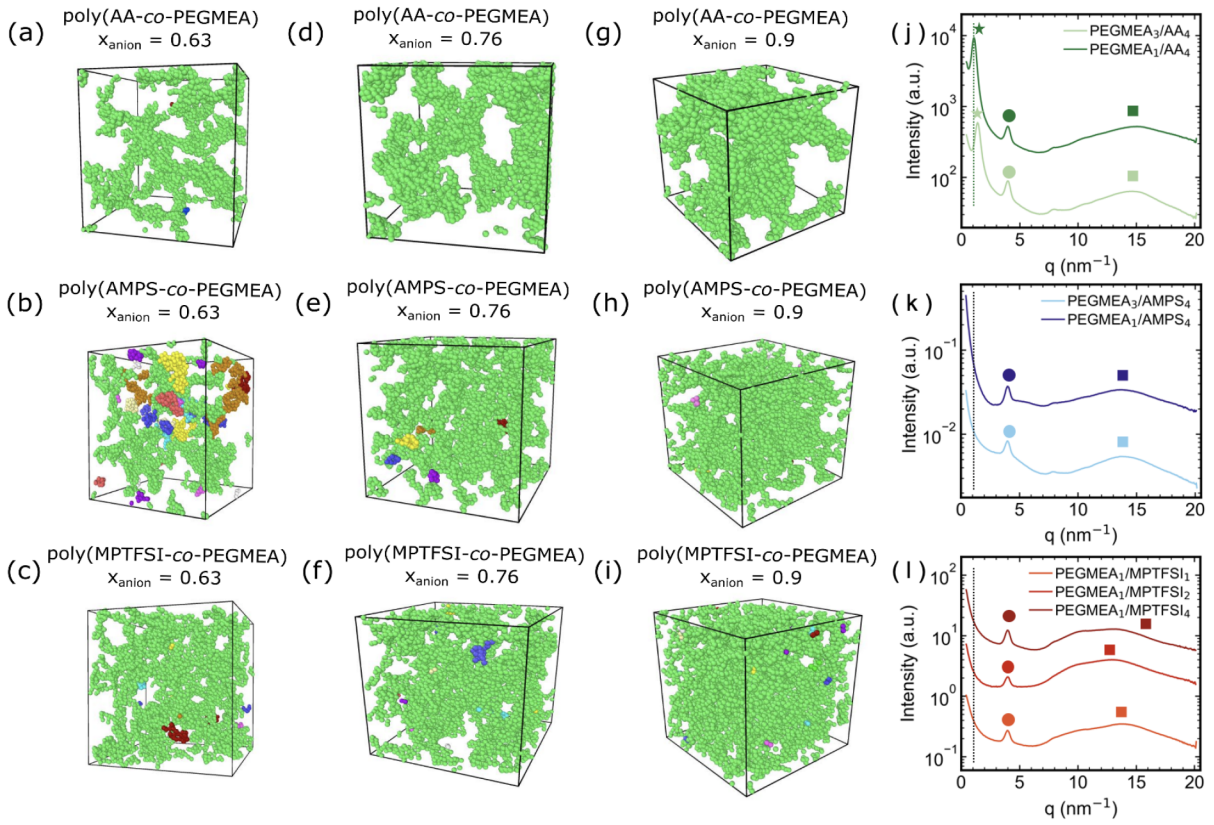

Figure 7. Morphological characteristics from simulations (a–i) and experiments (j–l) for electrolytes in the high ion content regime. (a–i) Snapshots of MD simulations at 600 K, showing only Li^+ ions and oxygens in the anionic groups. Different colors represent distinct aggregates. (j–l) X-ray scattering profiles from experiments at 300 K. The $I(q)$ plots are shifted vertically for clarity.

i), we noticed that the ion cluster morphologies containing AA differed significantly from those with AMPS or MPTFSI. The ions in the systems containing AMPS or MPTFSI organized into well-dispersed morphologies. In contrast, the ions in the AA-based electrolytes formed a separate ion-rich phase that was accompanied by a significant amount of "void" space. This morphological picture was characterized by a slow decay of the Li^+–Li^+ radial distribution functions in AA-containing electrolytes to the asymptotic value of one as shown in Figure 8. The similarly slow decay of Li^+–O(anion) and O(anion)–O(anion) radial distribution functions are also presented in Figures S16 and S17.

We collected X-ray scattering data for the electrolytes with high ion composition (Figure 7j–l) to corroborate the morphological observations from simulations. Lower ion composition scattering data is included in Figure S13. All electrolytes exhibited a primary scattering peak at $q = 4$ nm^{-1} (marked with circles, artifact of Kapton) and a broad scattering feature at $q \approx 12–15$ nm^{-1} (marked with squares) including an uncharged control (Figure S28). The scattering profiles for the AA-based electrolytes exhibit an additional scattering feature (marked with stars) at $q \approx 1–2$ nm^{-1}. The presence of the additional peak at lower q for the electrolytes containing AA was consistent with the scattering due to the phase-separated ionic domains. Furthermore, this peak shifted to larger length scales as the carboxylate fraction increased, suggesting an increase in the size of the ionic domains. These characteristics are in agreement with the simulated ionic morphologies (Figure 7a,d,g), which suggests significant phase separation of ions from the rest of the polymer backbones and PEGMEA side chains in electrolytes containing AA. The phase separation of ions from the rest of the polymer backbone and PEGMEA side chains may be due to the relatively stronger electrostatic interactions between the Li^+ and AA anions counteracting the formation of a homogeneous morphology. Similarly, the absence of the additional peaks in electrolytes containing AMPS or MPTFSI suggested negligible phase separation of ions, consistent with the corresponding simulated morphologies. On the basis of these results, we infer that the ionic aggregate morphologies for the AA-based electrolytes provides a continuous, percolated path for Li^+ with enhanced proximity of the hopping sites (Figure 8), leading to faster ion exchanges and higher diffusivities. This result demonstrates the importance of morphology in influencing the transport properties of comb-branched single-ion conducting materials.

Together, the results discussed in this section suggest that in the low ion content regime, both the Li^+ transport and ionic conductivity are slaved to the polymer dynamics. At such low ion concentrations, the electrolytes containing MPTFSI exhibited the highest decoupling of ion transport from polymer dynamics due to the relatively weaker electrostatic interactions of the Li^+-anion pair. At higher ion composition, the Li^+ transport was significantly faster than that for the polyanions due to the long-range movement of Li^+ ions by successive hopping along the large, percolated, immobile ionic aggregates. We further highlighted the unanticipated influence of ion-aggregate morphology on ion transport in the high ion concentration regime. Future design efforts for single-ion conducting comb-branched electrolytes may benefit from optimization of morphology rather than composition of the polymer alone.

https://doi.org/10.1021/acs.macromol.2c02500
Macromolecules 2023, 56, 2790–2800

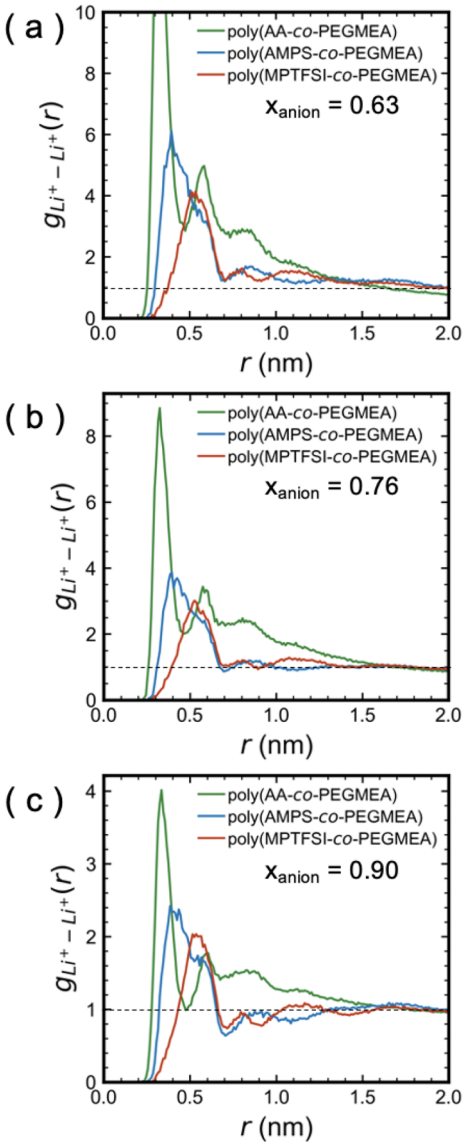

Figure 8. Simulated Li^+-Li^+ radial distribution functions for electrolytes with (a) $x_{anion} = 0.63$, (b) $x_{anion} = 0.76$, and (c) $x_{anion} = 0.9$. Systems with different anion chemistries are represented as AA (green), AMPS (blue), and MPTFSI (red).

CONCLUSIONS

In summary, a series of single-ion conducting electrolytes in a comb-branched architecture were synthesized by grafting-through poly(ethylene glycol) methyl ether acrylate and one of the three different lithiated anionic groups into a single copolymer backbone. The anion identity was found to significantly influence the ionic conductivity and the extent of decoupling of ionic conductivity from polymer segmental motion. At lower ion concentrations in the copolymer, the electrolytes containing MPTFSI were observed to exhibit both highest ionic conductivity and strongest degree of decoupling of ion transport from polymer dynamics. A monotonic increase in the activation energies for ion transport was observed on increasing the composition of anion in the copolymer, indicating potentially different mechanisms for ion transport at varying ion contents.

With the help of atomistic MD simulations, we report molecular level insights on the mechanisms underlying the ion transport characteristics. Our simulation results suggest that the Li^+ transport at lower ion concentrations is dictated by the codiffusion of Li^+−polymer pair and the rearrangement of ionic aggregates, resulting in comparable diffusivities for Li^+ and polyanions. In this regime, the highest degree of decoupling observed for the MPTFSI-containing electrolytes was attributed to the relatively weaker ion-pair electrostatic interaction. With increasing ion content, the ionic aggregates size increased resulting in decreased polymer mobility. At higher ion composition, the ionic aggregates percolate providing a continuous path for long-range Li^+ transport along the ionic aggregates. This results in single-ion conduction with considerably faster Li^+ transport compared to the polymer diffusion. We further highlight that in the high ion composition regime, the interplay between the resulting ionic aggregate morphologies and the strength of ion-pair electrostatic interactions, should guide the choice of counterion identity for achieving maximum ionic conductivity.

ASSOCIATED CONTENT

Supporting Information

The Supporting Information is available free of charge at https://pubs.acs.org/doi/10.1021/acs.macromol.2c02500.

Molecular dynamics model details including molecular architecture and electronic information of all atoms and bonds, simulation methodology, additional polymer characterization data including nuclear magnetic resonance spectra, dynamic scanning calorimetry traces, electrochemical impedance spectroscopy data (raw and fitted), and wide-angle X-ray scattering, advanced simulation data related to the ion dynamics in the system, and all simulation box renderings (PDF)

AUTHOR INFORMATION

Corresponding Authors

Nathaniel A. Lynd − *McKetta Department of Chemical Engineering, University of Texas at Austin, Austin, Texas 78712, United States;* orcid.org/0000-0003-3010-5068; Email: lynd@che.utexas.edu

Thomas M. Truskett − *McKetta Department of Chemical Engineering and Department of Physics, University of Texas at Austin, Austin, Texas 78712, United States;* orcid.org/0000-0002-6607-6468; Email: truskett@che.utexas.edu

Venkat Ganesan − *McKetta Department of Chemical Engineering, University of Texas at Austin, Austin, Texas 78712, United States;* orcid.org/0000-0003-3899-5843; Email: venkat@che.utexas.edu

Authors

Sanket Kadulkar − *McKetta Department of Chemical Engineering, University of Texas at Austin, Austin, Texas 78712, United States;* orcid.org/0000-0002-2834-7677

Zachary W. Brotherton − *McKetta Department of Chemical Engineering, University of Texas at Austin, Austin, Texas 78712, United States*

Anna L. Lynch − *Department of Chemistry, Smith College, Northampton, Massachusetts 01063, United States*

Gabriel Pohlman − *Department of Chemistry, Texas State University, San Marcos, Texas 78666, United States;* orcid.org/0000-0003-0044-3285

https://doi.org/10.1021/acs.macromol.2c02500
Macromolecules 2023, 56, 2790−2800

Zidan Zhang − *McKetta Department of Chemical Engineering, University of Texas at Austin, Austin, Texas 78712, United States;* orcid.org/0000-0002-6909-8742

Rudy Torres − *Walker Department of Mechanical Engineering, University of Texas at Austin, Austin, Texas 78712, United States;* orcid.org/0000-0002-5738-694X

Arumugam Manthiram − *Walker Department of Mechanical Engineering, University of Texas at Austin, Austin, Texas 78712, United States;* orcid.org/0000-0003-0237-9563

Complete contact information is available at: https://pubs.acs.org/10.1021/acs.macromol.2c02500

Author Contributions

#These authors contributed equally to this work.

Notes

The authors declare no competing financial interest.

■ ACKNOWLEDGMENTS

This research was primarily supported by the National Science Foundation through the Center for Dynamics and Control of Materials: an NSF MRSEC under Cooperative Agreement No. DMR-1720595. The authors acknowledge the Texas Advanced Computing Center (TACC) for providing computing resources that have contributed to the research results reported within this paper. We also acknowledge the Welch Foundation (Grant Nos. F-1599, F-1696, and F-1904) for support.

■ REFERENCES

(1) Chazalviel, J.-N. Electrochemical aspects of the generation of ramified metallic electrodeposits. *Phys. Rev. A* **1990**, *42*, 7355−7367.

(2) Armand, M.; Tarascon, J.-M. Building better batteries. *Nature* **2008**, *451*, 652−657.

(3) Diederichsen, K. M.; McShane, E. J.; McCloskey, B. D. Promising Routes to a High Li^+ Transference Number Electrolyte for Lithium Ion Batteries. *ACS Energy Lett.* **2017**, *2*, 2563−2575.

(4) Li, L.; Li, S.; Lu, Y. Suppression of dendritic lithium growth in lithium metal-based batteries. *Chem. Commun.* **2018**, *54*, 6648−6661.

(5) Zhu, J.; Zhang, Z.; Zhao, S.; Westover, A. S.; Belharouak, I.; Cao, P.-F. Single-Ion Conducting Polymer Electrolytes for Solid-State Lithium−Metal Batteries: Design, Performance, and Challenges. *Adv. Energy Mater.* **2021**, *11*, 2003836.

(6) Deng, K.; Zeng, Q.; Wang, D.; Liu, Z.; Qiu, Z.; Zhang, Y.; Xiao, M.; Meng, Y. Single-ion conducting gel polymer electrolytes: design, preparation and application. *J. Mater. Chem. A* **2020**, *8*, 1557−1577.

(7) Gao, J.; Wang, C.; Han, D.-W.; Shin, D.-M. Single-ion conducting polymer electrolytes as a key jigsaw piece for next-generation battery applications. *Chem. Sci.* **2021**, *12*, 13248−13272.

(8) Aziz, S. B.; Woo, T. J.; Kadir, M.; Ahmed, H. M. A conceptual review on polymer electrolytes and ion transport models. *Journal of Science: Advanced Materials and Devices* **2018**, *3*, 1−17.

(9) Xu, K. Electrolytes and Interphases in Li-Ion Batteries and Beyond. *Chem. Rev.* **2014**, *114*, 11503−11618.

(10) Hallinan, D. T.; Balsara, N. P. Polymer Electrolytes. *Annu. Rev. Mater. Research* **2013**, *43*, 503−525.

(11) Jeong, K.; Park, S.; Lee, S.-Y. Revisiting polymeric single lithium-ion conductors as an organic route for all-solid-state lithium ion and metal batteries. *J. Mater. Chem. A* **2019**, *7*, 1917−1935.

(12) Zhang, H.; Li, C.; Piszcz, M.; Coya, E.; Rojo, T.; Rodriguez-Martinez, L. M.; Armand, M.; Zhou, Z. Single lithium-ion conducting solid polymer electrolytes: advances and perspectives. *Chem. Soc. Rev.* **2017**, *46*, 797−815.

(13) Cao, C.; Li, Y.; Feng, Y.; Long, P.; An, H.; Qin, C.; Han, J.; Li, S.; Feng, W. A sulfonimide-based alternating copolymer as a single-ion polymer electrolyte for high-performance lithium-ion batteries. *J. Mater. Chem. A* **2017**, *5*, 22519−22526.

(14) Oh, H.; Xu, K.; Yoo, H. D.; Kim, D. S.; Chanthad, C.; Yang, G.; Jin, J.; Ayhan, I. A.; Oh, S. M.; Wang, Q. Poly(arylene ether)-Based Single-Ion Conductors for Lithium-Ion Batteries. *Chem. Mater.* **2016**, *28*, 188−196.

(15) Feng, S.; Shi, D.; Liu, F.; Zheng, L.; Nie, J.; Feng, W.; Huang, X.; Armand, M.; Zhou, Z. Single lithium-ion conducting polymer electrolytes based on poly[(4-styrenesulfonyl)-(trifluoromethanesulfonyl)imide] anions. *Electrochim. Acta* **2013**, *93*, 254−263.

(16) Meziane, R.; Bonnet, J.-P.; Courty, M.; Djellab, K.; Armand, M. Single-ion polymer electrolytes based on a delocalized polyanion for lithium batteries. *Electrochim. Acta* **2011**, *57*, 14−19. Polymer Electrolytes.

(17) Porcarelli, L.; Shaplov, A. S.; Salsamendi, M.; Nair, J. R.; Vygodskii, Y. S.; Mecerreyes, D.; Gerbaldi, C. Single-Ion Block Copoly(ionic liquid)s as Electrolytes for All-Solid State Lithium Batteries. *ACS Appl. Mater. & Inter.* **2016**, *8*, 10350−10359.

(18) Zhao, S.; Zhang, Y.; Pham, H.; Carrillo, J.-M. Y.; Sumpter, B. G.; Nanda, J.; Dudney, N. J.; Saito, T.; Sokolov, A. P.; Cao, P.-F. Improved Single-Ion Conductivity of Polymer Electrolyte via Accelerated Segmental Dynamics. *ACS Appl. Energy Mater.* **2020**, *3*, 12540−12548.

(19) Sun, X.-G.; Hou, J.; Kerr, J. B. Comb-shaped single ion conductors based on polyacrylate ethers and lithium alkyl sulfonate. *Electrochim. Acta* **2005**, *50*, 1139−1147.

(20) Cowie, J.; Spence, G. Novel single ion, comb-branched polymer electrolytes. *Solid State Ionics* **1999**, *123*, 233−242.

(21) Ren, C.; Liu, M.; Zhang, J.; Zhang, Q.; Zhan, X.; Chen, F. Solid-state single-ion conducting comb-like siloxane copolymer electrolyte with improved conductivity and electrochemical window for lithium batteries. *J. Appl. Polym. Sci.* **2018**, *135*, 45848.

(22) Zhao, S.; Song, S.; Wang, Y.; Keum, J.; Zhu, J.; He, Y.; Sokolov, A. P.; Cao, P.-F. Unraveling the Role of Neutral Units for Single-Ion Conducting Polymer Electrolytes. *ACS Appl. Mater. Interfaces* **2021**, *13*, 51525−51534.

(23) Abbott, L. J.; Lawson, J. W. Effects of Side Chain Length on Ionic Aggregation and Dynamics in Polymer Single-Ion Conductors. *Macromolecules* **2019**, *52*, 7456−7467.

(24) Frischknecht, A. L.; Paren, B. A.; Middleton, L. R.; Koski, J. P.; Tarver, J. D.; Tyagi, M.; Soles, C. L.; Winey, K. I. Chain and Ion Dynamics in Precise Polyethylene Ionomers. *Macromolecules* **2019**, *52*, 7939−7950.

(25) Buitrago, C. F.; Bolintineanu, D. S.; Seitz, M. E.; Opper, K. L.; Wagener, K. B.; Stevens, M. J.; Frischknecht, A. L.; Winey, K. I. Direct Comparisons of X-ray Scattering and Atomistic Molecular Dynamics Simulations for Precise Acid Copolymers and Ionomers. *Macromolecules* **2015**, *48*, 1210−1220.

(26) Hall, L. M.; Stevens, M. J.; Frischknecht, A. L. Dynamics of Model Ionomer Melts of Various Architectures. *Macromolecules* **2012**, *45*, 8097−8108.

(27) Bollinger, J. A.; Stevens, M. J.; Frischknecht, A. L. Quantifying Single-Ion Transport in Percolated Ionic Aggregates of Polymer Melts. *ACS Macro Lett.* **2020**, *9*, 583−587.

(28) Chen, X.; Chen, F.; Liu, M. S.; Forsyth, M. Polymer architecture effect on sodium ion transport in PSTFSI-based ionomers: A molecular dynamics study. *Solid State Ionics* 2016, *288*, 271−276, Proceedings of the 20th International Conference on Solid State Ionics SSI-20.

(29) Bolintineanu, D. S.; Stevens, M. J.; Frischknecht, A. L. Atomistic Simulations Predict a Surprising Variety of Morphologies in Precise Ionomers. *ACS Macro Lett.* **2013**, *2*, 206−210.

(30) Middleton, L. R.; Tarver, J. D.; Cordaro, J.; Tyagi, M.; Soles, C. L.; Frischknecht, A. L.; Winey, K. I. Heterogeneous Chain Dynamics and Aggregate Lifetimes in Precise Acid-Containing Polyethylenes: Experiments and Simulations. *Macromolecules* **2016**, *49*, 9176−9185.

(31) Gunday, S. T.; Kamal, A. Z.; Almessiere, M. A.; Çelik, S. U.; Bozkurt, A. An investigation of lithium ion conductivity of copolymers based on P(AMPS-co-PEGMA). *J. Appl. Polym. Sci.* **2019**, *136*, 47798.

(32) Evans, J.; Vincent, C. A.; Bruce, P. G. Electrochemical measurement of transference numbers in polymer electrolytes. *Polymer* **1987**, *28*, 2324−2328.

(33) Jorgensen, W. L.; Maxwell, D. S.; Tirado-Rives, J. Development and Testing of the OPLS All-Atom Force Field on Conformational Energetics and Properties of Organic Liquids. *J. Am. Chem. Soc.* **1996**, *118*, 11225−11236.
(34) Doherty, B.; Zhong, X.; Gathiaka, S.; Li, B.; Acevedo, O. Revisiting OPLS Force Field Parameters for Ionic Liquid Simulations. *J. Chem. Theory Comp.* **2017**, *13*, 6131−6145.
(35) Canongia Lopes, J. N.; Pádua, A. A. H.; Shimizu, K. Molecular Force Field for Ionic Liquids IV: Trialkylimidazolium and Alkoxycarbonyl-Imidazolium Cations; Alkylsulfonate and Alkylsulfate Anions. *J. Phys. Chem. B* **2008**, *112*, 5039−5046.
(36) Becke, A. D. Density-functional thermochemistry. III. The role of exact exchange. *J. Chem. Phys.* **1993**, *98*, 5648−5652.
(37) Lee, C.; Yang, W.; Parr, R. G. Development of the Colle-Salvetti correlation-energy formula into a functional of the electron density. *Phys. Rev. B* **1988**, *37*, 785−789.
(38) Krishnan, R.; Binkley, J. S.; Seeger, R.; Pople, J. A. Self-consistent molecular orbital methods. XX. A basis set for correlated wave functions. *J. Chem. Phys.* **1980**, *72*, 650−654.
(39) Frisch, M. J. et al. *Gaussian˜16* Revision C.01. 2016; Gaussian Inc.: Wallingford CT.
(40) Plimpton, S. Fast Parallel Algorithms for Short − Range Molecular Dynamics. *J. Comput. Phys.* **1995**, *117*, 1−19.
(41) Diederichsen, K. M.; Buss, H. G.; McCloskey, B. D. The Compensation Effect in the Vogel−Tammann−Fulcher (VTF) Equation for Polymer-Based Electrolytes. *Macromolecules* **2017**, *50*, 3831−3840.
(42) Zhang, Z.; Wheatle, B. K.; Krajniak, J.; Keith, J. R.; Ganesan, V. Ion Mobilities, Transference Numbers, and Inverse Haven Ratios of Polymeric Ionic Liquids. *ACS Macro Lett.* **2020**, *9*, 84−89.
(43) Fong, K. D.; Self, J.; McCloskey, B. D.; Persson, K. A. Onsager Transport Coefficients and Transference Numbers in Polyelectrolyte Solutions and Polymerized Ionic Liquids. *Macromolecules* **2020**, *53*, 9503−9512.
(44) Hall, L. M.; Seitz, M. E.; Winey, K. I.; Opper, K. L.; Wagener, K. B.; Stevens, M. J.; Frischknecht, A. L. Ionic Aggregate Structure in Ionomer Melts: Effect of Molecular Architecture on Aggregates and the Ionomer Peak. *J. Am. Chem. Soc.* **2012**, *134*, 574−587.
(45) Castagna, A. M.; Wang, W.; Winey, K. I.; Runt, J. Structure and Dynamics of Zinc-Neutralized Sulfonated Polystyrene Ionomers. *Macromolecules* **2011**, *44*, 2791−2798.
(46) Sevick, E. M.; Monson, P. A.; Ottino, J. M. Monte Carlo calculations of cluster statistics in continuum models of composite morphology. *J. Chem. Phys.* **1988**, *88*, 1198−1206.

https://doi.org/10.1021/acs.macromol.2c02500
Macromolecules 2023, 56, 2790−2800